EUROPEAN ORGANIZATION FOR NUCLEAR RESEARCH

CERN-PH-EP/2006-032
3 October 2006

Measurement of the branching ratios of the decays $\Xi^0 \to \Sigma^+ e^- \overline{\nu}_e$ and $\overline{\Xi^0} \to \overline{\Sigma^+} e^+ \nu_e$

NA48/1 Collaboration

J.R. Batley, G.E. Kalmus[1)], C. Lazzeroni, D.J. Munday, M. Patel, M.W. Slater, S.A. Wotton

Cavendish Laboratory, University of Cambridge, Cambridge, CB3 0HE, UK[2)]

R. Arcidiacono, G. Bocquet, A. Ceccucci, D. Cundy[3)], N. Doble[4)], V. Falaleev, L. Gatignon, A. Gonidec, P. Grafström, W. Kubischta, F. Marchetto[5)], I. Mikulec[6)], A. Norton, B. Panzer-Steindel, P. Rubin[7)], H. Wahl[8)]

CERN, CH-1211 Genève 23, Switzerland

E. Goudzovski, P. Hristov[9)], V. Kekelidze, L. Litov, D. Madigozhin, N. Molokanova, Yu. Potrebenikov, S. Stoynev, A. Zinchenko

Joint Institute for Nuclear Research, Dubna, Russian Federation

E. Monnier[10)], E.C. Swallow[11)], R. Winston[12)]

The Enrico Fermi Institute, The University of Chicago, Chicago, Illinois, 60126, U.S.A.

R. Sacco[13)], A. Walker

Department of Physics and Astronomy, University of Edinburgh, JCMB King's Buildings, Mayfield Road, Edinburgh, EH9 3JZ, U.K.

W. Baldini, P. Dalpiaz, P.L. Frabetti, A. Gianoli, M. Martini, F. Petrucci, M. Scarpa, M. Savrié

Dipartimento di Fisica dell'Università e Sezione dell'INFN di Ferrara, I-44100 Ferrara, Italy

A. Bizzeti[14)], M. Calvetti, G. Collazuol[15)], E. Iacopini, M. Lenti, G. Ruggiero[9)], M. Veltri[16)]

Dipartimento di Fisica dell'Università e Sezione dell'INFN di Firenze, I-50125 Firenze, Italy

M. Behler, K. Eppard, M. Eppard[9)], A. Hirstius[9)], K. Kleinknecht, U. Koch, L. Masetti, P. Marouelli, U. Moosbrugger, C. Morales Morales, A. Peters[9)], R. Wanke, A. Winhart

Institut für Physik, Universität Mainz, D-55099 Mainz, Germany[17)]

A. Dabrowski, T. Fonseca Martin[9)], M. Velasco

Department of Physics and Astronomy, Northwestern University, Evanston Illinois 60208-3112, U.S.A.

G. Anzivino, P. Cenci, E. Imbergamo, G. Lamanna[18)], P. Lubrano, A. Michetti, A. Nappi, M. Pepe, M.C. Petrucci, M. Piccini[9)], M. Valdata

Dipartimento di Fisica dell'Università e Sezione dell'INFN di Perugia, I-06100 Perugia, Italy

C. Cerri, F. Costantini, R. Fantechi, L. Fiorini[19)], S. Giudici, I. Mannelli, G. Pierazzini, M. Sozzi

Dipartimento di Fisica, Scuola Normale Superiore e Sezione dell'INFN di Pisa, I-56100 Pisa,

Italy

C. Cheshkov, J.B. Cheze, M. De Beer, P. Debu, G. Gouge, G. Marel, E. Mazzucato, B. Peyaud, B. Vallage

DSM/DAPNIA - CEA Saclay, F-91191 Gif-sur-Yvette, France

M. Holder, A. Maier, M. Ziolkowski

Fachbereich Physik, Universität Siegen, D-57068 Siegen, Germany[20)]

C. Biino, N. Cartiglia, M. Clemencic, S. Goy Lopez, E. Menichetti, N. Pastrone

Dipartimento di Fisica Sperimentale dell'Università e Sezione dell'INFN di Torino, I-10125 Torino, Italy

W. Wislicki,

Soltan Institute for Nuclear Studies, Laboratory for High Energy Physics, PL-00-681 Warsaw, Poland[21)]

H. Dibon, M. Jeitler, M. Markytan, G. Neuhofer, L. Widhalm

Österreichische Akademie der Wissenschaften, Institut für Hochenergiephysik, A-10560 Wien, Austria[22)]

Submitted for publication in Physics Letters B.

[1)] Present address: Rutherford Appleton Laboratory, Chilton, Didcot, OX11 0QX, UK

[2)] Funded by the U.K. Particle Physics and Astronomy Research Council

[3)] Present address: Instituto di Cosmogeofisica del CNR di Torino, I-10133 Torino, Italy

[4)] Also at Dipartimento di Fisica dell'Università e Sezione dell'INFN di Pisa, I-56100 Pisa, Italy

[5)] On leave from Sezione dell'INFN di Torino, I-10125 Torino, Italy

[6)] On leave from Österreichische Akademie der Wissenschaften, Institut für Hochenergiephysik, A-1050 Wien, Austria

[7)] On leave from University of Richmond, Richmond, VA, 23173, USA; supported in part by the US NSF under award #0140230. Present address: Department of Physics and Astronomy George Mason University, Fairfax, VA 22030A, USA

[8)] Also at Dipartimento di Fisica dell'Università e Sezione dell'INFN di Ferrara, I-44100 Ferrara, Italy

[9)] Present address: CERN, CH-1211 Genève 23, Switzerland

[10)] Present address: Centre de Physique des Particules de Marseille, IN2P3-CNRS, Université de la Méditerranée, Marseille, France

[11)] Present address: Department of Physics, Elmhurst College, Elmhurst, IL, 60126, USA

[12)] Also at University of California, Merced, USA

[13)] Present address: Department of Physics Queen Mary, University of London, Mile End Road, London E1 4NS, United Kingdom

[14)] Dipartimento di Fisica dell'Università di Modena e Reggio Emilia, via G. Campi 213/A I-41100, Modena, Italy

[15)] Present address: Scuola Normale Superiore e Sezione dell'INFN di Pisa, I-56100 Pisa, Italy

[16)] Istituto di Fisica, Università di Urbino, I-61029 Urbino, Italy

[17)] Funded by the German Federal Minister for Research and Technology (BMBF) under contract 7MZ18P(4)-TP2

[18)] Present address: Dipartimento di Fisica e Sezione dell'INFN di Pisa, I-56100 Pisa, Italy

[19)] Present address: Cavendish Laboratory, University of Cambridge, Cambridge, CB3 0HE, U.K.

[20)] Funded by the German Federal Minister for Research and Technology (BMBF) under contract 056SI74

[21)] Supported by the Committee for Scientific Research grants 5P03B10120, SPUB-M/CERN/P03/DZ210/2000 and SPB/CERN/P03/DZ146/2002

[22)] Funded by the Austrian Ministry for Traffic and Research under the contract GZ 616.360/2-IV GZ 616.363/2-VIII, and by the Fonds für Wissenschaft und Forschung FWF Nr. P08929-PHY

Abstract

From 56 days of data taking in 2002, the NA48/1 experiment observed 6316 $\Xi^0 \to \Sigma^+ e^- \overline{\nu}_e$ candidates (with the subsequent $\Sigma^+ \to p\pi^0$ decay) and 555 $\overline{\Xi^0} \to \overline{\Sigma^+} e^+ \nu_e$ candidates with background contamination of 215 ± 44 and 136 ± 8 events, respectively. From these samples, the branching ratios $\mathrm{BR}(\Xi^0 \to \Sigma^+ e^- \overline{\nu}_e) = (2.51 \pm 0.03_{\mathrm{stat}} \pm 0.09_{\mathrm{syst}}) \times 10^{-4}$ and $\mathrm{BR}(\overline{\Xi^0} \to \overline{\Sigma^+} e^+ \nu_e) = (2.55 \pm 0.14_{\mathrm{stat}} \pm 0.10_{\mathrm{syst}}) \times 10^{-4}$ were measured allowing the determination of the CKM matrix element $|V_{\mathrm{us}}| = 0.209^{+0.023}_{-0.028}$. Using the Particle Data Group average for $|V_{\mathrm{us}}|$ obtained in semileptonic kaon decays, we measured the ratio $g_1/f_1 = 1.20 \pm 0.05$ of the axial-vector to vector form factors.

1 Introduction

The study of hadron β-decays gives important information on the interplay between the weak interaction and the hadronic structure determined by the strong interaction. This information is richer for baryon than for meson semileptonic decays owing to the presence of three valence quarks as opposed to a quark-antiquark pair. In this context, Ξ^0 β-decay represents an extraordinary opportunity to test, by analogy with neutron β-decay, SU(3) symmetry and, through the determination of V_{us}, the quark mixing model [1].

In the exact SU(3) symmetry approximation, the ratio between the axial-vector form factor g_1 and the vector form factor f_1 for Ξ^0 β-decay is equal to the one for the decay $n \to p e^- \overline{\nu}_e$. Theoretical models that incorporate SU(3) symmetry breaking effects give predictions which, however, differ significantly from each other [2, 3, 4, 5, 6, 7, 8, 9]. Precise tests of SU(3) symmetry breaking effects calculations in semileptonic hyperon decays are therefore important in connection with the determination of V_{us}, independently from kaon decays.

Recently, the KTeV experiment has obtained the first determination of the g_1/f_1 ratio in $\Xi^0 \to \Sigma^+ e^- \overline{\nu}_e$ decays from the study of the Σ^+ polarization with the decay $\Sigma^+ \to p\pi^0$ and the $e^- - \overline{\nu}_e$ correlation [10]. Their result, based on the observation of 487 events, is consistent with exact SU(3) symmetry: $g_1/f_1 = 1.32^{+0.21}_{-0.17\mathrm{stat}} \pm 0.05_{\mathrm{syst}}$. Previously, the same Collaboration published the value of the branching ratio $\mathrm{BR}(\Xi^0 \to \Sigma^+ e^- \overline{\nu}_e) = (2.71 \pm 0.22_{\mathrm{stat}} \pm 0.31_{\mathrm{syst}}) \times 10^{-4}$ from a sample of 176 events after background subtraction [11].

In the present work, the Ξ^0 and $\overline{\Xi^0}$ β-decay modes have been investigated with significantly improved statistics as compared to previous experiments. The corresponding branching ratios were determined relative to the decay channels $\Xi^0 \to \Lambda\pi^0$ and $\overline{\Xi^0} \to \overline{\Lambda}\pi^0$, respectively, allowing the measurement of the matrix element $|V_{\mathrm{us}}|$. Conversely, using as input parameter the current experimental value for V_{us} from semileptonic kaon decays, the form factor g_1/f_1 was determined.

2 Beam and detector

The main goal of the NA48/1 experiment is the study of very rare K_S decay modes and neutral hyperon decays. A detailed description of the beam line and the detector can be found in [12]. Only the aspects relevant to this measurement are reviewed here.

2.1 Beam

The experiment was performed at the CERN SPS accelerator and used a 400 GeV/c proton beam impinging on a Be target to produce a neutral beam. The spill length was

4.8 s out of a 16.2 s cycle time. The proton intensity was fairly constant during the spill with a mean of 5×10^{10} particles per pulse.

For this measurement, only the K_S target station of the NA48 double K_S/K_L beam line [12] was used to produce the neutral beam. In this configuration, the K_L beam was blocked and an additional sweeping magnet was installed to deflect charged particles away from the defining section of the K_S collimators. To reduce the number of photons in the neutral beam originating primarily from π^0 decays, a 24 mm thick platinum absorber was placed in the beam between the target and the collimator. A pair of coaxial collimators, having a total thickness of 5.1 m, the axis of which formed an angle of 4.2 mrad to the proton beam direction, selected a beam of neutral long-lived particles (K_S, K_L, Λ^0, Ξ^0, n and γ). The aperture of the defining collimator, 5.03 m downstream of the target, was a circle with 1.8 mm radius. The target position and the production angle where chosen in such a way that the beam axis was hitting the center of the electromagnetic calorimeter.

In order to minimize the interaction of the neutral beam with air, the collimator was immediately followed by a 90 m long evacuated tank terminated by a 0.3% X_0 thick Kevlar window. The NA48 detector was located downstream of this region in order to collect the products of the particles decaying in the volume contained by the tank.

On average, about 1.4×10^4 Ξ^0 per spill, with an energy between 70 and 220 GeV, decayed in the fiducial decay volume.

2.2 Tracking

The detector included a spectrometer housed in a helium gas volume with two drift chambers before (DCH1, DCH2) and two after (DCH3, DCH4) a dipole magnet with a horizontal transverse momentum kick of 265 MeV/c. Each chamber had four views (*x, y, u, v*), each of which had two sense wire planes. In DCH1, DCH2 and DCH4, all wire planes were instrumented while in the drift chamber located just downstream of the magnet (DCH3), only vertical and horizontal wire planes were read out. The resulting space points were reconstructed with a resolution of about 150 μm in each projection. The spectrometer momentum resolution could be parameterized as:

$$\sigma_p/p = 0.48\% \oplus 0.015\% \times p \tag{1}$$

where p is in GeV/c. This resulted in a resolution of about 1 MeV/c^2 when reconstructing the Λ mass in $\Lambda \to p\pi^-$ decays. The track time resolution was about 1.4 ns.

2.3 Calorimetry

The electromagnetic showers were detected and measured with a 27 radiation-length deep liquid krypton calorimeter (LKr) read out in longitudinal cells with a $\sim 2 \times 2$ cm^2 cross-section.

The energy resolution was given by [13]:

$$\sigma(E)/E = \frac{3.2\%}{\sqrt{E}} \oplus \frac{9\%}{E} \oplus 0.42\% \tag{2}$$

where E is in GeV. The transverse position resolution for a single photon of energy larger than 20 GeV was better than 1.3 mm and the corresponding mass resolution at the π^0 mass was about 1 MeV/c^2. The time resolution of the calorimeter for a single shower was better than 300 ps.

A scintillating fiber hodoscope (NHOD), placed inside the LKr calorimeter at a depth of about 9.5 X_0 near the shower maximum, was used for trigger efficiency measurements.

The LKr calorimeter was followed by a hadron calorimeter (HAC) consisting of an iron-scintillator sandwich, 6.7 nuclear interaction lengths thick. The HAC provided a raw measurement of the energy for hadron showers and it was only used at the first trigger level.

2.4 Scintillator Detectors

A scintillator hodoscope (CHOD) was located between the spectrometer and the calorimeter. It consisted of two planes, segmented in horizontal and vertical strips and arranged in four quadrants. The CHOD time resolution was better than 200 ps for 2-track events. Muon counters made of three planes of scintillator, each shielded by an iron wall, were placed at the downstream end of the apparatus. Seven rings of scintillation counters (AKL), placed around the evacuated decay volume and around the helium tank of the charged particle spectrometer, were used to veto activity outside the acceptance region of the detector determined by the LKr calorimeter.

3 Trigger

The trigger system used for the on-line selection of Ξ^0 β-decays consisted of three levels of logic. Level 1 (L1) was based on logic combinations of fast signals coming from various sub-detectors. It required hits in the CHOD and in the first drift chamber compatible with at least one and two tracks respectively, no hit in the AKL veto system and a minimum energy deposition in the calorimeters. This last requirement was 15 GeV for the energy reconstructed in the LKr calorimeter or 30 GeV for the summed energy in the electromagnetic and hadronic calorimeters. The output rate of the L1 stage was about 50 kHz. The average L1 efficiency, measured with $\Xi^0 \to \Lambda\pi^0$ events of energy greater than 70 GeV, was found to be $98.65 \pm 0.03\%$.

Level 2 (L2) consisted of 300 MHz processors that reconstructed tracks and vertices from hits in the drift chambers and computed relevant physical quantities. The L2 trigger required at least two tracks with a closest distance of approach of less than 8 cm in space and a transverse separation greater than 5 cm in the first drift chamber. Since the signature of the Ξ^0 β-decay involves the detection of an energetic proton from the subsequent $\Sigma^+ \to p\pi^0$ decay, the ratio between the higher and the lower of the two track momenta was required to be larger than 3.5. Rejection of the overwhelming $\Lambda \to p\pi^-$ and $K_S \to \pi^+\pi^-$ decays was achieved by applying stringent invariant mass cuts according to the corresponding event hypotheses, $p\pi$ or $\pi\pi$ (see Fig. 1). The output L2 trigger rate was about 2.5 kHz. The efficiency of the L2 trigger stage with respect to Level 1, averaged over the 2002 run, was measured to be $(83.7 \pm 2.1)\%$ for Ξ^0 β-decays, mainly limited by wire inefficiencies in the drift chambers.

The L2 trigger output rate was further reduced by about a factor 2 at Level 3 (L3). The L3 trigger consisted of a farm of computers which used a specialized version of the off-line reconstruction code. It combined track measurements with clusters in the LKr calorimeter and used loose selection criteria. The inefficiency of the L3 trigger was measured to be less than 0.1%. For normalization and efficiency determination purposes, the L3 trigger also received events from downscaled L1 triggers as well as from NHOD pulses.

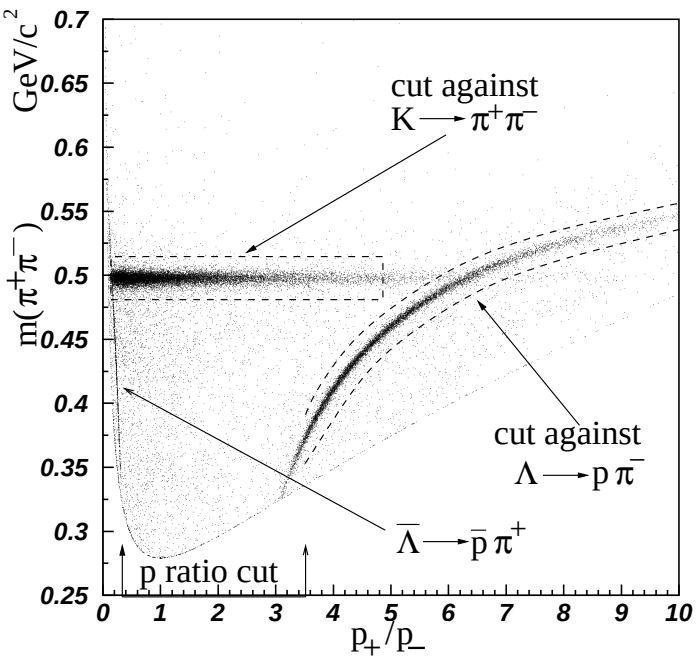

Figure 1: Reconstructed $\pi^+\pi^-$ invariant mass versus momentum ratio of positive to negative particles for 2-track vertices as selected by the L1 trigger. Events coming from $K_S \to \pi^+\pi^-$ and $\Lambda \to p\pi^-$ decays are clearly visible. $\overline{\Lambda} \to \overline{p}\pi^+$ decays are located in the $p_+/p_- < 0.3$ region. The kinematical regions rejected by the L2 trigger are also shown.

4 Event selection and background rejection

4.1 $\Xi^0 \to \Sigma^+ e^- \overline{\nu}_e$

The identification of the $\Xi^0 \to \Sigma^+ e^- \overline{\nu}_e$ channel was performed using the subsequent decay $\Sigma^+ \to p\pi^0$ with $\pi^0 \to \gamma\gamma$. The final state consisted of a proton and an electron leaving tracks in the spectrometer in addition to two photons being detected as clusters in the LKr calorimeter and one unobserved anti-neutrino. The decay $\Xi^0 \to \Sigma^+ \ell^- \overline{\nu}_e$ is the only source of Σ^+ particles in the neutral beam since the two-body decay $\Xi^0 \to \Sigma^+ \pi^-$ is kinematically forbidden. Thus, the signal events were identified by requiring an invariant $p\pi^0$ mass consistent with the nominal Σ^+ mass value.

The two tracks were required to be less than 2 ns apart in time, measured by the charged hodoscope or by the drift chambers when the hodoscope readout was not able to reconstruct the track time. This occurred for about 2% of the events, mainly due to the presence of double-pulses from the scintillator photomultipliers. To suppress contamination from accidental activity in the detector, events with an additional track within a time window of 20 ns with respect to the average time of the signal tracks were rejected.

The lower momentum thresholds for positive and negative tracks were set to 40 GeV/c and 4 GeV/c, respectively (Fig. 2(a) and Fig. 3(a)). The momentum ratio between positive and negative tracks was required to be greater than 4.5 and the distance between the impact points of the two tracks in the first chamber was chosen to be greater than 12 cm in order to reduce biases from the corresponding cuts applied by L2. To ensure full efficiency in the track reconstruction, the radial distance to the beam axis of the reconstructed space points in the drift chambers had to lie between 12.5 cm and 110 cm.

Electron identification was achieved by calculating the ratio E/p of the cluster energy in the LKr calorimeter associated to the track with the measured momentum in the spectrometer. Since electrons deposited their total energy in the electromagnetic calorimeter, their E/p ratio was required to be between 0.85 and 1.15. For protons, the E/p value was required to be less than 0.8. To avoid shower overlap, a minimum transverse distance of at least 15 cm was imposed between track impact points on the calorimeter surface.

The distance between the two tracks at the point of closest approach had to be less than 3 cm. In order to minimize the background coming from $\Xi^0 \to \Lambda\pi^0$ decays with $\Lambda \to p\pi^-$ and π^- misidentified as electron, the difference between the nominal Λ mass and the reconstructed invariant mass of the two tracks under the $p\pi^-$ hypothesis had to be greater than 14 MeV/c^2. Background from $K_S \to \pi^+\pi^-$ decays with one accidental π^0 or two accidental photons was suppressed by rejecting events with an invariant $\pi^+\pi^-$ mass within 30 MeV/c^2 of the nominal kaon mass and with a momentum ratio less than 6. The last three selection criteria were tighter than the ones used in the trigger to reduce biases from L2 trigger inefficiencies.

The two-photon clusters forming a neutral pion candidate had to be within a time window of 2 ns and the energy of each cluster was required to be in the 3-100 GeV range. The reconstructed π^0 energy distribution is shown in Fig. 2(b). Inner and outer regions of the LKr calorimeter were excluded by requiring the radial distance to the beam axis of each cluster to be between 15 cm and 110 cm. Moreover, the center of each cluster was required to be at a distance greater than 2 cm from any dead calorimeter cell. To avoid biases in the energy measurement of the photons due to shower contamination induced by other particles, their associated clusters had to have a minimal distance from other clusters measured within a time window of 5 ns. This minimal separation was set to 10 cm for electron and photon candidates and to 25 cm for hadronic showers associated with proton tracks. Photons originating from bremsstrahlung produced in the detector material before the magnet were rejected by measuring the separation at the LKr location between clusters and the impact point of the extrapolated upstream segment of a track.

The Σ^+ decay was reconstructed using a positive charged track in the spectrometer and two clusters in the electromagnetic calorimeter within a time window of 2 ns. The longitudinal position of the Σ^+ decay vertex was determined using the π^0 mass constraint to calculate the distance of its decay point from the calorimeter:

$$\Delta z_{\pi^0} = \frac{1}{m_{\pi^0}} \sqrt{E_1 E_2 r_{12}^2} \tag{3}$$

where E_1, E_2 are the energies and r_{12} the distance between the two clusters in the transverse plane of the calorimeter. The transverse position of the vertex was then obtained by extrapolating back the proton track to the longitudinal position of the π^0 decay point. The momentum vector of the decaying Σ^+ particle was calculated from the proton track parameters, the photon energies and assuming the emitted photons originate from the reconstructed vertex.

The Ξ^0 decay vertex position was obtained by computing the closest distance of approach between the extrapolated Σ^+ line-of-flight and the electron track. This distance was required to be less than 4 cm. Furthermore, the deviation of the transverse Ξ^0 vertex position from the nominal line-of-flight defined by a straight line going from the center of the K_S target to the center of the liquid krypton calorimeter was required to be less than 3 cm.

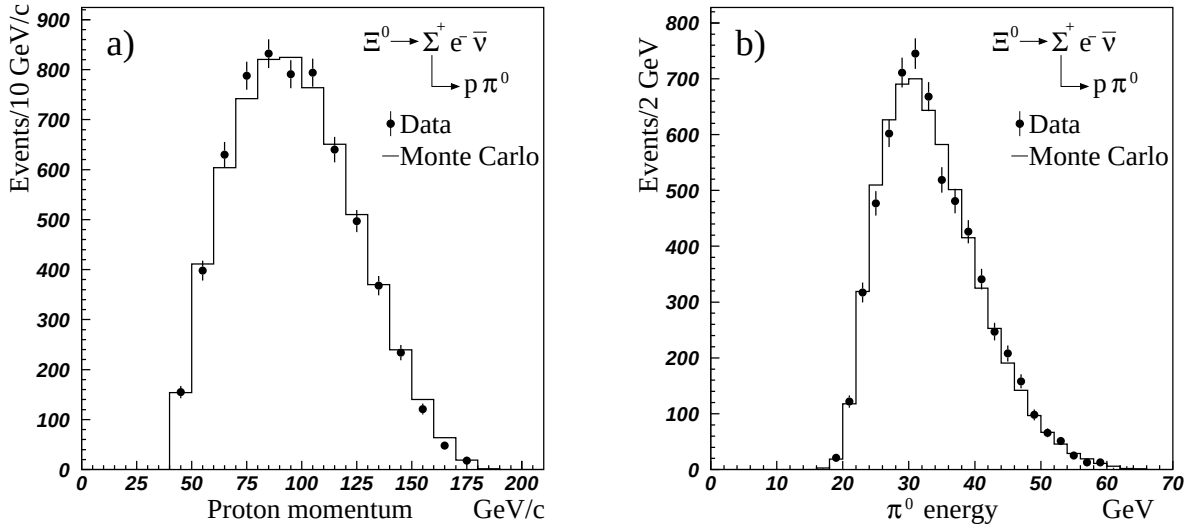

Figure 2: Reconstructed proton momentum (a) and π^0 energy (b) distributions for $\Xi^0 \to \Sigma^+ e^- \overline{\nu}_e$ events with the subsequent $\Sigma^+ \to p\pi^0$ decay.

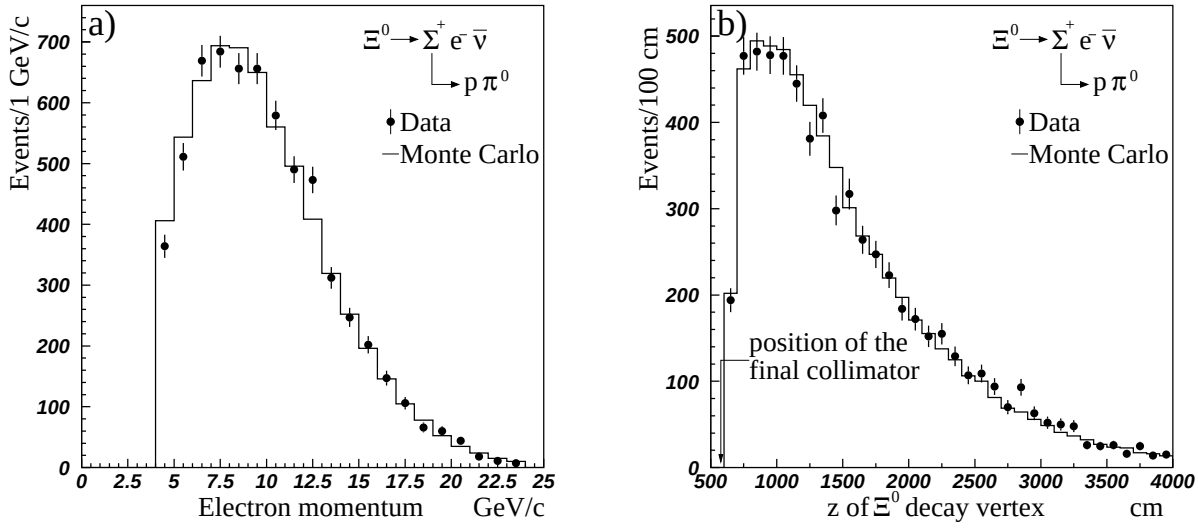

Figure 3: Reconstructed electron momentum (a) and z-vertex coordinate (b) distributions for $\Xi^0 \to \Sigma^+ e^- \overline{\nu}_e$ events.

The longitudinal position of the Ξ^0 vertex was required to be at least 6.5 m downstream of the K_S target, i.e. 0.5 m after the end of the final collimator and at most 40 m from the target (see Fig. 3(b)). Similarly, the Σ^+ vertex position was required to be at least 6.5 m downstream of the target but at most 50 m from the target. The latter value was chosen larger than the upper limit for the Ξ^0 vertex position to account for the lifetime of the Σ^+ particle. The longitudinal separation between the Ξ^0 and Σ^+ decay vertices was required to be between -8 m and 40 m. The negative lower limit, tuned with Monte Carlo events, was chosen such as to take properly into account resolution effects.

The quantity $\vec{r}_{\rm COG}$ was defined as $\vec{r}_{\rm COG} = \sum_i \vec{r}_i E_i / \sum_i E_i$ where E_i is the energy of the detected particle and $\vec{r}_i$ the corresponding transverse position vector at the liquid krypton calorimeter position z_{LKr}. For a charged particle, the quantity $\vec{r}_i$ was obtained from the extrapolation to z_{LKr} of the upstream segment of the associated track. The quantity $|\vec{r}_{\rm COG}|$ had to be less than 15 cm. This requirement was found to produce negligible losses of signal events since the undetected neutrino in the Ξ^0 β-decay carries only a small fraction of the Ξ^0 energy.

Good candidates were kept if their $p\pi^0$ invariant mass was found to be within $8\,{\rm MeV/c^2}$ of the nominal Σ^+ mass value, corresponding to a mass window of ± 4 standard deviations. Finally, the visible Ξ^0 energy was required to be in the 70 to 220 GeV range. In the rare case that after all cuts were applied more than one candidate was found (more than one pair of photons associated to two tracks satisfying the event selection), the one with the smallest closest distance of approach between the Σ^+ line-of-flight and the electron track was chosen.

With the above selection criteria, 6316 $\Xi^0 \to \Sigma^+ e^- \overline{\nu}_e$ candidates were observed in the signal region. The distribution of events in the $p\pi^0$ invariant mass variable is shown in Fig. 4 after all selection cuts were applied. Signal events peaking around the Σ^+ mass are clearly identified and well separated from the abundant $\Xi^0 \to \Lambda\pi^0$ decays (with $\Lambda \to pe^-\overline{\nu}_e$) located at low-mass values. Monte-Carlo studies showed that contamination in the signal region from such events was negligible. Other background sources like $K_L \to \pi^+\pi^-\pi^0$ decays or $\Xi^0 \to \Lambda\pi^0$ followed by $\Lambda \to p\pi^-$ with mis-identified charged pions were also found not to contribute significantly. An amount of $(2.2 \pm 0.2)\%$ of background events in the signal region was estimated from the linear extrapolation of the distribution of events in the mass side-bands. By studying the time distribution of events in side-bands regions, about 20% only of this background was attributed to residual accidental activity while most of the remaining contribution could be accounted for by re-scattering particles in the collimator, not rejected by the $|\vec{r}_{\rm COG}| < 15\,{\rm cm}$ selection cut. An additional source of unwanted events was associated with the production of Ξ^0s in the final collimator. Such events, although mostly present at large $|\vec{r}_{\rm COG}|$ values, exhibit a peak in the $p\pi^0$ invariant mass distribution, consistent with the Σ^+ mass (see Fig. 5). Although these events are genuine $\Xi^0 \to \Sigma^+ e^- \overline{\nu}_e$ decays, they were subtracted from the final sample in order to minimize uncertainties associated with their production yield and acceptance calculation. From inspection of the $|\vec{r}_{\rm COG}|$ distribution of events in the Σ^+ mass region, a contribution of $(1.2 \pm 0.7)\%$ of Ξ^0 β-decays originating from the final collimator was estimated, yielding a total background contamination in the signal region of $(3.4 \pm 0.7)\%$.

4.2 $\Xi^0 \to \Lambda\pi^0$

To minimize systematic uncertainties in the branching ratio measurement, the selection of the normalization events $\Xi^0 \to \Lambda\pi^0$ with $\Lambda \to p\pi^-$ and $\pi^0 \to \gamma\gamma$ was performed with analysis criteria as similar to the signal channel as possible. In particular, the same

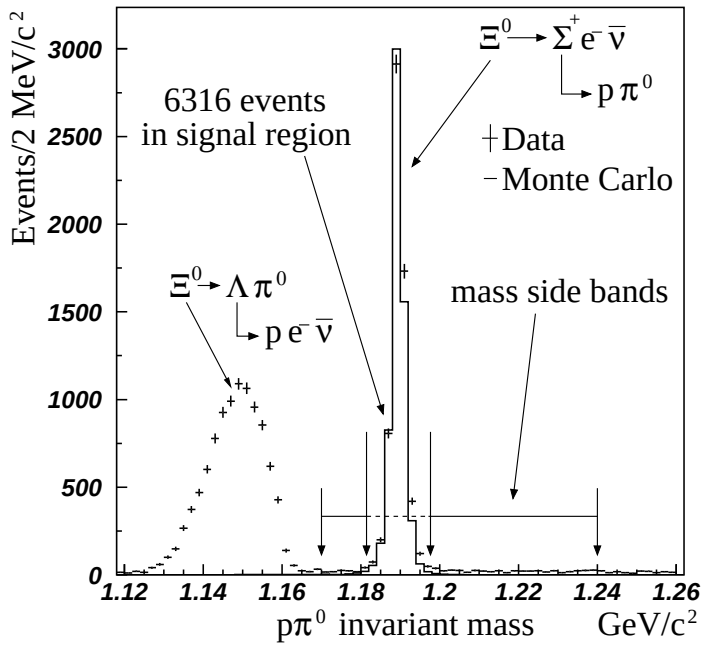

Figure 4: Reconstructed $p\pi^0$ invariant mass distribution for $\Xi^0 \to \Sigma^+ e^- \overline{\nu}_e$ candidates after all selection criteria were applied. The solid line shows the Monte Carlo prediction for the signal. The peak at the Σ^+ mass value shows clear evidence for the signal.

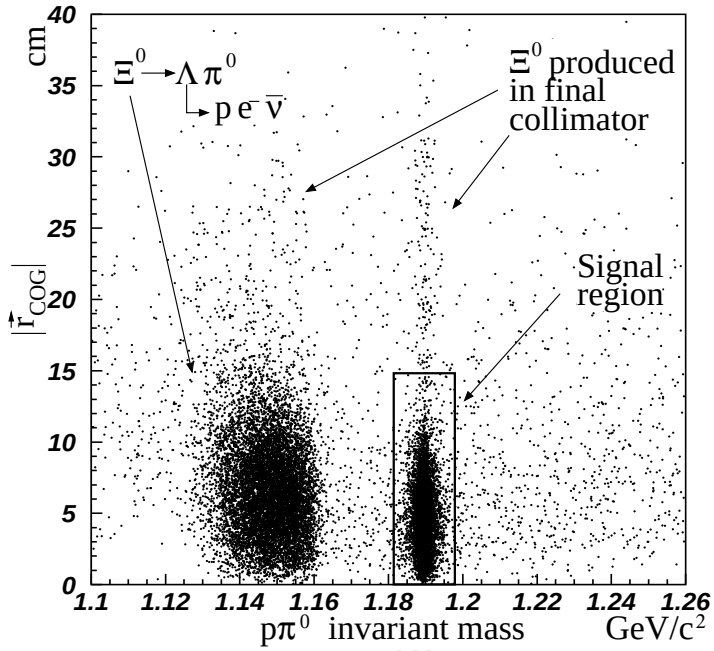

Figure 5: Scatter plot of $|\vec{r}_{\rm COG}|$ versus the $p\pi^0$ invariant mass for events passing all other selection cuts. Events extending to high $|\vec{r}_{\rm COG}|$ values and centered around the Σ^+ mass are due to Ξ^0s produced in the final collimator.

sensitive detector volume definition and time requirements for tracks and clusters were used.

For the π^- selection, the minimum momentum threshold was set to 5 GeV/c and no E/p cut was applied. Since the proton and the negatively charged pion originate from a vertex (Λ decay), the closest distance of approach between the two tracks was required to be less than 2.2 cm. The reconstructed invariant $p\pi^-$ mass was required to be within 4 MeV/c^2 of the nominal Λ mass. The position of the Λ decay vertex was required to be at least 6.5 m downstream of the target but at most 50 m from the target. As $\Xi^0 \to \Lambda\pi^0$ decays are fully reconstructed in the detector, the upper value of the energy center-of-gravity was reduced to 7 cm.

The longitudinal position of the $\Xi^0 \to \Lambda\pi^0$ decay point was defined by the π^0 vertex as in the case of the Ξ^0 β-decay by applying the same procedure for the vertex reconstruction. The fiducial volume of the decay was contained longitudinally between 6.5 m and 40 m from the K_S target and the Ξ^0 energy was required to be in the 70-220 GeV range (see Fig. 6 (a)). Finally, the reconstructed $\Lambda\pi^0$ mass was required to be within the range 1.31 to 1.32 GeV/c^2. This mass window corresponds to about four standard deviations around the nominal Ξ^0 mass (see Fig. 6(b)).

588798 candidates were observed in the signal region with a contamination of $(0.6 \pm 0.4)\%$ from Ξ^0s produced in the final collimator. After correcting for the average downscaling factor of 33.79 applied to the L1 control trigger, the corresponding number of $\Xi^0 \to \Lambda\pi^0$ normalization events in the fiducial decay region was 1.990×10^7.

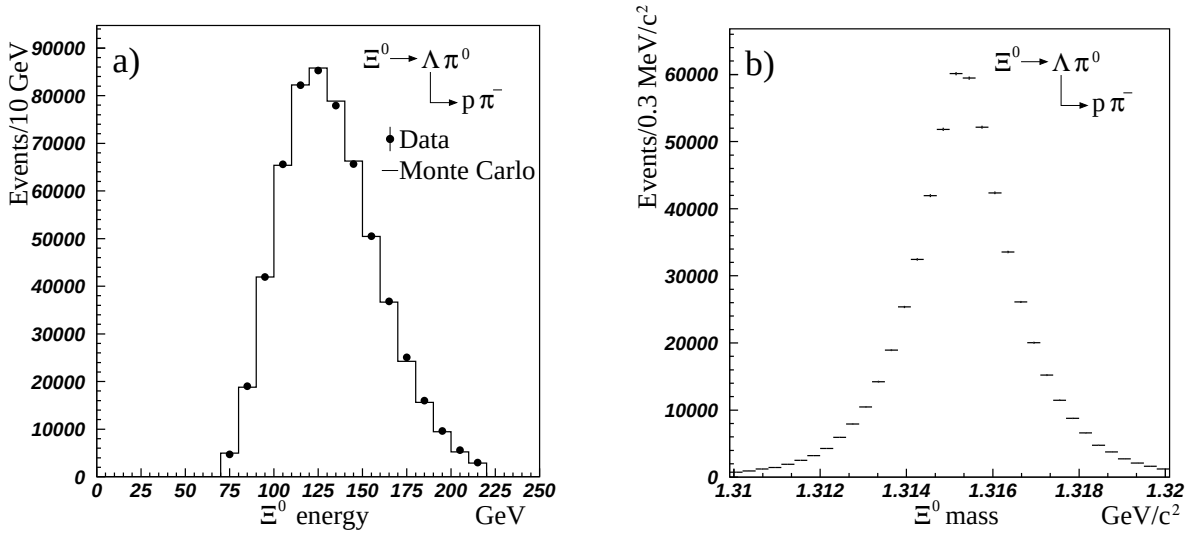

Figure 6: (a) Reconstructed Ξ^0 energy and (b) $\Lambda\pi^0$ invariant mass distributions for $\Xi^0 \to \Lambda\pi^0$ events.

5 Acceptance

The acceptance for both signal and normalization decay channels was computed using a detailed Monte Carlo program based on GEANT3 [12, 14]. Particle interactions in the detector material as well as the response functions of the different detector elements were taken into account in the simulation.

5.1 $\Xi^0 \to \Sigma^+ e^- \overline{\nu}_e$

The V-A transition matrix element for the decay $\Xi^0 \to \Sigma^+ e^- \overline{\nu}_e$ can be written as [15]:

$$M = \frac{V_{\rm us} G_F}{\sqrt{2}} [\bar{u}_{\Sigma^+} H_\mu u_{\Xi^0}][\bar{u}_e L^\mu u_\nu] + h.c. \tag{4}$$

where $V_{\rm us}$ is the appropriate CKM matrix element for $|\Delta S|$=1 transitions, G_F the Fermi coupling constant, $\bar{u}_{\Xi^0}$, $\bar{u}_e$, u_ν and u_{Σ^+} are Dirac spinors corresponding to the initial and final state particles. $\bar{u}_e L^\mu u_\nu$ is the matrix element of the leptonic weak current where L^μ has the well-established form

$$L^\mu = \gamma^\mu (1 + \gamma_5) \tag{5}$$

and $\bar{u}_{\Sigma^+} H_\mu u_{\Xi^0}$ is the contribution coming from the hadronic weak current. The calculation of this term would require the treatment of strong interaction effects. In practice, these are taken into account by introducing form factors in a parameterization of the most general form, compatible with Lorentz covariance:

$$H_\mu = (O_\mu^V + O_\mu^A) \tag{6}$$

with

$$O_\mu^V = f_1(q^2)\gamma_\mu + \frac{f_2(q^2)}{m_{\Xi^0}} \sigma_{\mu\nu} q^\nu + \frac{f_3(q^2)}{m_{\Xi^0}} q_\mu \tag{7}$$

$$O_\mu^A = \left(g_1(q^2)\gamma_\mu + \frac{g_2(q^2)}{m_{\Xi^0}} \sigma_{\mu\nu} q^\nu + \frac{g_3(q^2)}{m_{\Xi^0}} q_\mu \right) \gamma_5 \tag{8}$$

In the expressions above, $f_1(q^2)$, $f_2(q^2)$ and $f_3(q^2)$ are the form-factors associated to the vector component of the hadronic weak current while $g_1(q^2)$, $g_2(q^2)$ and $g_3(q^2)$ correspond to the axial vector part. The momentum transfer q^2, written in terms of the four-momenta of the involved particles, is:

$$q^\alpha = (p_e + p_\nu)^\alpha = (p_{\Xi^0} - p_{\Sigma^+})^\alpha \tag{9}$$

From the ingredients above, the $\Xi^0 \to \Sigma^+ e^- \overline{\nu}_e$ differential decay rate for a polarized initial hyperon beam could be calculated (for details, see [15, 16, 17]).

In the Monte Carlo simulation, we followed the prescription used in [15] in which terms including the f_3 (scalar) and g_3 (pseudo-scalar) form-factors were neglected since they are suppressed in the transition amplitude by a factor m_e/m_{Ξ^0}. In addition, the axial-tensor g_2 form-factor was set to 0 as second class currents are forbidden in the Standard Model. The values of the remaining non-vanishing form-factors f_1, g_1 and f_2 were obtained, with the assumption of SU(3) and CVC (conserved vector current) validity, from the available data on neutron β-decay and the nucleon magnetic moments [18, 19]:

$$\begin{aligned} f_1(0) &= 1 \\ f_2(0)/f_1(0) = \frac{m_{\Xi^0}}{m_n}\frac{(\mu_p - \mu_n)}{2} &= 2.5966 \pm 0.0004 \\ g_1(0)/f_1(0) &= 1.2695 \pm 0.0029, \end{aligned} \tag{10}$$

where μ_p and μ_n are the proton and neutron anomalous magnetic moments, respectively. The above values for g_1/f_1 and f_2/f_1 are in good agreement with the ones directly measured from Ξ^0 β-decays by the KTeV experiment [10]:

$$\begin{aligned} g_1/f_1 &= 1.32^{+0.21}_{-0.17\text{stat}} \pm 0.05_{\text{syst}} \\ f_2/f_1 &= 2.0 \pm 1.2_{\text{stat}} \pm 0.5_{\text{syst}} \end{aligned} \tag{11}$$

While f_2 was assumed constant, a dipole dependence as a function of the square of the momentum transfer was used for the f_1 and g_1 form-factors [15, 16]:

$$f_1(q^2) = f_1(0)(1 + 2\frac{q^2}{M_V^2}) \tag{12}$$

$$g_1(q^2) = g_1(0)(1 + 2\frac{q^2}{M_A^2}) \tag{13}$$

with $M_V = (0.97 \pm 0.04)$ GeV/c^2 and $M_A = (1.25 \pm 0.15)$ GeV/c^2 [16, 19, 20].

The polarization of the Ξ^0 beam depends on both the hyperon production angle and its momentum fraction with respect to the incoming proton beam. Since the Ξ^0 polarization was not measured in this experiment, an estimated value of -10% was used in the acceptance calculation. This amount is close to the preliminary measurement obtained by the KTeV experiment [21] for which the expected Ξ^0 polarization was comparable to the one in NA48/1.

The subsequent $\Sigma^+ \to p\pi^0$ decay was simulated according to the well-known angular distribution for spin-1/2 hyperons decaying into a spin-1/2 baryon and a pion [22]:

$$\frac{d\Gamma}{d\Omega} = \frac{1}{4\pi}(1 + \alpha_{\Sigma^+}\, \vec{P}_{\Sigma^+} \cdot \hat{e}) \tag{14}$$

where $\vec{P}_{\Sigma^+}$ is the polarization vector of the decaying Σ^+, $\hat{e}$ is the direction of the outgoing proton and $\alpha_{\Sigma^+} = 0.980^{+0.017}_{-0.015}$ [18] is the corresponding asymmetry parameter of the decay.

Radiative corrections to the differential decay rate were included following the prescription of [16] in which model-independent contributions to first order in α from virtual and inner-bremsstrahlung graphs are taken into account in the transition amplitude.

The acceptance for the Ξ^0 β-decays in the fiducial decay region was calculated to be $(2.492 \pm 0.009)\%$, where the quoted uncertainty originates from the statistics of the Monte Carlo sample. The inclusion of radiative corrections was found to increase the acceptance by 0.3%.

5.2 $\Xi^0 \to \Lambda\pi^0$

The generation of the normalization events $\Xi^0 \to \Lambda\pi^0$ with $\Lambda \to p\pi^-$ was performed using for each decay mode the form of the angular distribution given by Eq. 14 with the appropriate values for the polarization vectors and asymmetry parameters. The Λ polarization vector was obtained from the following relation:

$$\vec{P}_\Lambda = \frac{(\alpha_{\Xi^0} + \vec{P}_{\Xi^0} \cdot \hat{e}) \cdot \hat{e} + \beta_{\Xi^0} \cdot (\vec{P}_{\Xi^0} \times \hat{e}) + \gamma_{\Xi^0} \cdot \hat{e} \times (\vec{P}_{\Xi^0} \times \hat{e})}{1 + \alpha_{\Xi^0}\vec{P}_{\Xi^0} \cdot \hat{e}} \tag{15}$$

where $\hat{e}$ is the direction of the outgoing Λ, $\vec{P}_{\Xi^0}$ the polarization vector of the initial hyperon and α_{Ξ^0}= -0.411, β_{Ξ^0}=0.327 and γ_{Ξ^0}=0.85 are the asymmetry parameters used in the simulation for the $\Xi^0 \to \Lambda\pi^0$ [18]. For the non-leptonic $\Lambda \to p\pi^-$ channel, the value $\alpha_\Lambda = 0.642$ [18] was used.

The acceptance for the normalization $\Xi^0 \to \Lambda\pi^0$ events in the fiducial decay region was found to be $(1.377 \pm 0.004)\%$, assuming a polarization of -10% for the initial Ξ^0. The quoted uncertainty on the acceptance is again purely statistical.

6 $\Xi^0 \to \Sigma^+ e^- \overline{\nu}_e$ branching ratio

The determination of the $\Xi^0 \to \Sigma^+ e^- \overline{\nu}_e$ branching ratio was obtained from the background subtracted number of good events for signal and normalization, the corresponding acceptance values, the L2 trigger efficiency measured with respect to the L1 one and the normalization branching ratios [18]. These quantities are summarized in Table 1 and yield:

$$\mathrm{BR}(\Xi^0 \to \Sigma^+ e^- \overline{\nu}_e) = (2.51 \pm 0.03_{\mathrm{stat}} \pm 0.09_{\mathrm{syst}}) \times 10^{-4} \tag{16}$$

where the statistical uncertainty originates from the event statistics and the systematic one is the sum in quadrature of the various contributions presented in Table 2. This result

Table 1: Parameters used for the $\mathrm{BR}(\Xi^0 \to \Sigma^+ e^- \overline{\nu}_e)$ measurement.

	$\Xi^0 \to \Sigma^+ e^- \overline{\nu}_e$	$\Xi^0 \to \Lambda\pi^0$
Event statistics	6316	588798
Downscaling factor	1	33.79
Background	$(3.4 \pm 0.7)\%$	$(0.6 \pm 0.4)\%$
Acceptance	$(2.492 \pm 0.009)\%$	$(1.377 \pm 0.004)\%$
L2/L1 trigger efficiency	$(83.7 \pm 2.1)\%$	
$\mathrm{BR}(\Sigma^+ \to p\pi^0)$	$(51.57 \pm 0.30)\%$	
$\mathrm{BR}(\Xi^0 \to \Lambda\pi^0)$		$(99.523 \pm 0.013)\%$
$\mathrm{BR}(\Lambda \to p\pi^-)$		$(63.9 \pm 0.5)\%$

is in good agreement with existing measurements [11].

The largest contribution to the total systematic uncertainty comes from the L2 trigger efficiency whose determination was limited in precision by the statistics available in the control samples. The sensitivity of the branching ratio measurement to the form factors was studied by varying f_2/f_1 and g_1/f_1 within the limits provided by the uncertainties on M_V, M_A masses and on the $f_2(0)/f_1(0)$, $g_1(0)/f_1(0)$ parameters (Eq. 11), and was found to be mainly dominated by the precision on g_1.

Other systematic uncertainties due to acceptance and selection criteria were estimated to be 1.0% by varying the geometrical and kinematical cuts applied in the event selection. In particular, the sensitivity of the branching measurement to the inner radius cut in the first drift chamber was investigated. Since in both signal and normalization channels the outgoing protons carry a large part of the primary Ξ^0 energy, an important fraction of them travels along the detector near the beam pipe, in a region where the spectrometer efficiency and acceptance may change rapidly. The corresponding systematic uncertainty obtained from the variation of the measured branching ratio as a function of the inner radius cut in the first drift chamber was estimated not to exceed 0.6%.

Table 2: Sources of systematic uncertainties.

Source	uncertainty
Background	$\pm 0.8\%$
MC statistics	$\pm 0.5\%$
L2 trigger efficiency	$\pm 2.2\%$
Form factors	$\pm 1.6\%$
Geometrical and kinematical cuts	$\pm 1.0\%$
Ξ^0 polarization	$\pm 1.0\%$
Ξ^0 lifetime	$\pm 0.2\%$
Normalization	$\pm 1.0\%$
Total	$\pm 3.4\%$

Finally, an uncertainty of $\pm 5\%$ in the polarization of the initial Ξ^0 was assumed, resulting in a contribution of 1.0% to the systematic uncertainty on the $\Xi^0 \to \Sigma^+ e^- \overline{\nu}_e$ branching ratio.

7 $\overline{\Xi^0} \to \overline{\Sigma^+} e^+ \nu_e$ decays

Since the trigger system did not distinguish between particle charges with respect to the event hypotheses, the recorded data sample also contained decays of anti-hyperons, allowing the first measurement of the $\overline{\Xi^0} \to \overline{\Sigma^+} e^+ \nu_e$ branching ratio to be performed. Events originating from $\overline{\Xi^0} \to \overline{\Lambda}\pi^0$ decays were used as the normalization channel. In order to minimize systematic differences between the branching ratio determinations for Ξ^0 and $\overline{\Xi^0}$ β-decays, the same selection criteria for both modes were applied with the exception of the required charge inversion for tracks. Fig. 7(a) shows the $\overline{p}\pi^0$ invariant mass distribution of events after all other cuts were applied. A sample of 555 $\overline{\Xi^0} \to \overline{\Sigma^+} e^+ \nu_e$ candidates was found in the signal region with a background contamination of 136 ± 8 events, measured from the extrapolation of the flat distribution of events in the side-band regions around the $\overline{\Sigma^+}$ mass and taking into account possible contributions from $\overline{\Xi^0}$s produced in the final collimator. For the normalization channel $\overline{\Xi^0} \to \overline{\Lambda}\pi^0$, 47351 events with negligible background were identified using data samples obtained from control triggers. After taking into account the downscaling factors applied to the recorded data, the corresponding number of $\overline{\Xi^0} \to \overline{\Lambda}\pi^0$ events in the fiducial decay region was found to be 1.601×10^6.

The acceptance calculation was performed using Monte Carlo samples that were generated with the same matrix element as for the study of Ξ^0 β-decays and with a production energy spectrum adjusted to fit the spectrum of observed $\overline{\Xi^0} \to \overline{\Lambda}\pi^0$ events (see Fig. 7(b)). The $\overline{\Xi^0}$ production polarization was set to zero, as expected for anti-hyperons, and the signs of the decay parameters for both signal and normalization channels were changed according to the theory. The acceptance was found to be 1.80% for the $\overline{\Xi^0} \to \overline{\Sigma^+} e^+ \nu_e$ decay mode and 1.19% for the normalization channel, with negligible statistical uncertainties.

The L2 trigger is the main component of the trigger which affects the semileptonic $\overline{\Xi^0}$ branching ratio measurement. Due to the limited number of reconstructed $\overline{\Xi^0}$ events from control triggers, the L2 trigger efficiency was assumed to be the same as for Ξ^0 β-decays. However, an additional systematic uncertainty of 2.0% was added in quadrature in order to account for possible effects due to the different $\overline{\Xi^0}$ polarization value and production spectrum.

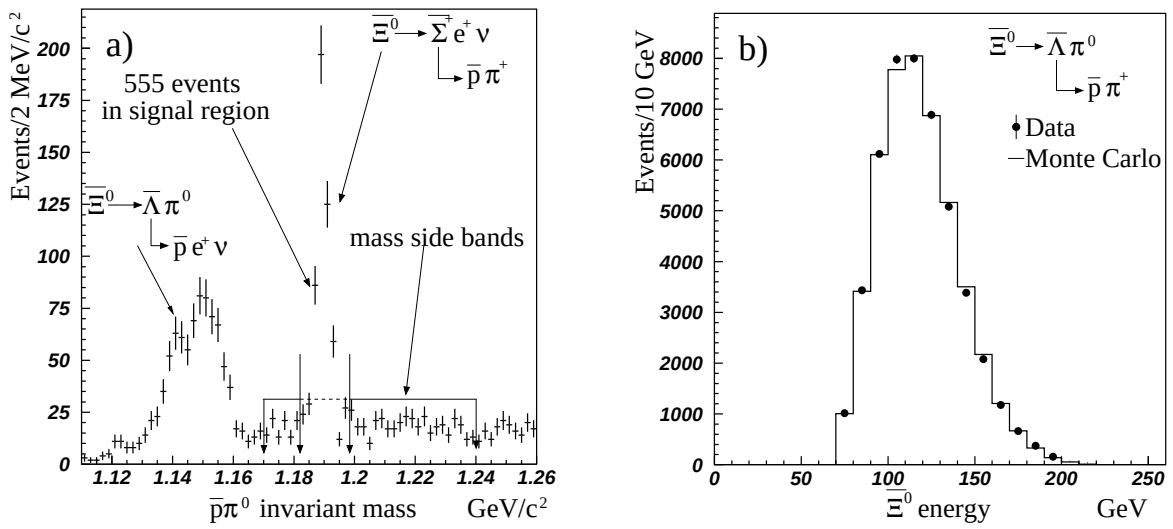

Figure 7: (a) $\overline{\mathrm{p}}\pi^0$ invariant mass distribution of events. The peak corresponding to the $\overline{\Sigma^+}$ mass shows clear evidence for $\overline{\Xi^0}$ β-decays. (b) $\overline{\Xi^0}$ energy distribution from $\overline{\Xi^0} \to \overline{\Lambda}\pi^0$ events.

The branching ratio for $\overline{\Xi^0} \to \overline{\Sigma^+}e^+\nu_e$ decays was measured to be:

$$\mathrm{BR}(\overline{\Xi^0} \to \overline{\Sigma^+}e^+\nu_e) = (2.55 \pm 0.14_{\mathrm{stat}} \pm 0.10_{\mathrm{syst}}) \times 10^{-4} \tag{17}$$

in very good agreement with the value obtained above for Ξ^0 β-decays. The relative systematic uncertainty of 3.9% is dominated by the trigger efficiency determination. Contributions to the systematic uncertainty from form factors, geometrical cuts and acceptance, rescattering effects in the final collimator as well as normalization were obtained from the study of the semileptonic Ξ^0 decay.

8 Determination of $|V_{\mathrm{us}}|$ and g_1/f_1

The $|V_{\mathrm{us}}|$ parameter can be extracted from the measured Ξ^0 semileptonic decay rates using the following relation [16]:

$$\begin{aligned}\Gamma = \frac{BR_{\Xi^0\to\Sigma e\nu}}{\tau_{\Xi^0}} =& G_F^2|V_{\mathrm{us}}|^2\frac{\Delta m^5}{60\pi^3}(1+\delta_{\mathrm{rad}}^{\mathrm{MD}})(1+\delta_{\mathrm{rad}}^{\mathrm{MI}}) \\ &\times\left\{(1-\frac{3}{2}\beta)(|f_1^2|+3|g_1^2|)+\frac{6}{7}\beta^2(|f_1^2|+2|g_1^2|+Re(f_1f_2^*)+\frac{2}{3}|f_2^2|)\right. \\ &\left.+\,\delta_{q^2}(f_1,g_1)\right\}\end{aligned} \tag{18}$$

where $\tau_{\Xi^0} = (2.90 \pm 0.09) \times 10^{-10}$ s is the Ξ^0 lifetime, $\Delta m = m_{\Xi^0} - m_{\Sigma^+} = 0.12546 \pm 0.00021$ GeV/c^2 and $\beta = \frac{\Delta m}{m_{\Xi^0}} = 0.09542 \pm 0.00011$ [18], $\delta_{\mathrm{rad}}^{\mathrm{MD}} = 0.0211$ and $\delta_{\mathrm{rad}}^{\mathrm{MI}} = 0.0226$ are, respectively, model-dependent and model-independent radiative corrections and $\delta_{q^2}(f_1, g_1) = 0.119$ takes into account the contribution from the transfer momentum dependence of the form-factors f_1 and g_1 [16]. Eq. 18 was computed neglecting terms of $O(\beta^3)$.

Using the combined result $BR_{\Xi^0\to\Sigma e\nu} = (2.51 \pm 0.09) \times 10^{-4}$ of the measured Ξ^0 and $\overline{\Xi^0}$ branching ratios together with the current experimental determination of g_1/f_1 and f_2/f_1 [10] and neglecting SU(3) breaking corrections to f_1, the value for $|V_{\rm us}|$ was found to be

$$|V_{\rm us}| = 0.209^{+0.023}_{-0.028} \ , \tag{19}$$

consistent with the present value obtained from kaon semileptonic decays [18]. The uncertainty on $|V_{\rm us}|$ is dominated by the experimental precision on g_1/f_1, and the corresponding contribution due to the branching ratio measurement itself is now comparable to the error on the Ξ^0 lifetime.

Conversely, the g_1/f_1 ratio could be extracted from Eq. 18 using the current $V_{\rm us}$ value obtained from kaon decays [18]:

$$g_1/f_1 = 1.20 \pm 0.04_{\rm br} \pm 0.03_{\rm ext} \tag{20}$$

where the uncertainty coming from the present branching ratio measurement (br) takes into account the weak dependence of the acceptance on g_1/f_1 itself. The external error (ext) includes the contributions from $V_{\rm us}$, Ξ^0 lifetime and f_2/f_1 uncertainties. Our measurement is in agreement with exact SU(3) symmetry and favours theoretical approaches in which SU(3) breaking effects do not modify significantly the g_1/f_1 ratio.

9 Conclusion

Using the data collected in 2002 with the NA48 detector at CERN, we obtained the first determination of the $\overline{\Xi^0} \to \overline{\Sigma^+} e^+ \nu_e$ branching ratio and performed a measurement of the $\Xi^0 \to \Sigma^+ e^- \overline{\nu}_e$ branching ratio with a precision significantly better than the existing published values. Our results provide, in addition, a new determination of the ratio g_1/f_1 or, alternatively, of the $|V_{\rm us}|$ parameter.

Acknowledgments

It is a pleasure to thank the technical staff of the participating laboratories, universities and affiliated computing centers for their efforts in the construction of the NA48 apparatus, in the operation of the experiment, and in the processing of the data.

References

[1] N. Cabibbo, Physical Review Letters 10 (1963) 531.
[2] J.F. Donoghue,B.R. Holstein, S.W. Klimt Phys. Rev. D 35: (1987) 934.
[3] L.J. Carson, R.J. Oakes, C.R. Willcox, Physical Review D 37 (1988) 3197.
[4] A. Krause, Helv. Phys. Acta 63 (1990) 3.
[5] J. Anderson and M.A. Luty, Phys. Rev. D 47 (1993) 4975.
[6] F. Schlumpf, Phys. Rev. D 51 (1995) 2262.
[7] R. Flores-Mendieta, A. Garcia and G. Sanchez-Colon, Phys.Rev. D54 (1996) 6855.
[8] R. Flores-Mendieta, E. Jenkins and A.V. Manohar, Phys. Rev. D 58 (1998) 094028.
[9] P. G. Ratcliffe, Phys. Rev. D 59 (1999) 014038.
[10] A. Alavi-Harati et al., Physical Review Letters 87 (2001) 132001.
[11] A. Affolder et al., Physical Review Letters 82 (1999) 3751. See also A. Alavi-Harati, Proceedings to "Batavia 1999, Hyperon physics" (1999) 60.
[12] J.R. Batley et al., Physics Letters B 544 (2002) 97.
[13] G. Unal, NA48 Collaboration, IX International Conference on Calorimetry, October 2000, Annecy, France, hep-ex/0012011.

[14] GEANT Description and Simulation Tool, CERN Program Library Long Writeup, W5013 (1994) 1.
[15] N. Cabibbo, E.C. Swallow, R. Winston, Annual Review of Nuclear and Particle Science, 55 (2003) 39.
[16] A. Garcia, P. Kielanowski, Lecture Notes in Physics Vol. 222, Springer-Verlag, Berlin, (1985) 1.
[17] V. Linke, Nuclear Physics B 12 (1969) 669.
[18] W.M. Yao et al., Particle Data Book 2006, Journal of Physics G 33 (2006) 1.
[19] M. Gaillard and G. Sauvage, Ann. Rev. Nucl. Part. Sci. 34 (1984) 351.
[20] A.M. Cnops et al., Oxford Neutrino Conference (1978) 62.
[21] T. Alexopoulos, A. Erwin, Proceedings to Batavia 1999, Hyperon physics (1999) 48.
[22] E. D. Commins, P. H. Bucksbaum,"Weak interactions of leptons and quarks", Cambridge University Press (1983).